Supplementary Material

Spin Waves in Ferrimagnets near the Angular Magnetization Compensation Temperature: A Micromagnetic Study

Luis Sánchez-Tejerina, David Osuna Ruiz, Eduardo Martínez, Luis López Díaz, Víctor Raposo, and Óscar Alejos

S1 Micromagnetic Model

In this section we describe the micromagnetic model in which the numerical solver is based, giving the expression for the energy desnity and the effective field considered, as well as the expression of the spin-orbit torque (SOT).

As stated in the main text, micromagnetic simulations have been carried out with a homemade code[16–18] modelling the FiM material as formed by two sub-lattices coupled through an interlattice exchange interaction. Accordingly, a pair of coupled Landau-Lifshitz-Gilbert equations are used to model the material:[16–18]

$$\dot{\mathbf{m}}_i = -\gamma_i \mathbf{m}_i \times \mathbf{H}_{\text{eff},i} + \alpha_i \mathbf{m}_i \times \dot{\mathbf{m}}_i + \tau_{\text{SOT},i} \qquad (i = 1,2), \tag{S1}$$

where $\mathbf{m}_i$, γ_i and α_i are the local orientation of the magnetization, the gyromagnetic factor, and the damping parameter for each sub-lattice, respectively, and $\tau_{\text{SOT},i} = \gamma_i \frac{\hbar \theta_{SH}}{2et\mu_0 M_{s,i}} J\, \mathbf{m} \times (\mathbf{m} \times \boldsymbol{\sigma})$ corresponds to the spin-orbit torque (SOT) due to spin currents. In the last expression $\hbar$ is the reduced Planck constant, θ_{SH} the spin Hall angle measuring the electric current to spin current conversion efficiency, e the elementary charge, t the layer thickness, μ_0 the vacuum magnetic permeability, $M_{s,i}$ the sublattice saturation magnetization, and J the applied current density which induce a spin accumulation along $\boldsymbol{\sigma} = \mathbf{u}_y$. The coupling of this two equations is given through the effective field, $\mathbf{H}_{\text{eff},i}$, defined as the variational derivative of the energy density, $\mathbf{H}_{\text{eff},i} = -\frac{1}{\mu_0 M_{s,i}} \frac{\delta \varepsilon}{\delta \mathbf{m}_i}$. The energy density ε includes all relevant interactions within the system, being the exchange, anisotropy and interfacial Dzyaloshinkii-Moriya interactions:

$$\varepsilon = \varepsilon_{exch} + \varepsilon_{anis} + \varepsilon_{dmi}. \tag{S2}$$

In this work, we have considered a uniaxial anisotropy along the direction perpendicular to a thin film slab as sketched in Fig. S1(a), being the anisotropy constant, $K_{u,i}$ the same for both sublattices

$$\varepsilon_{anis} = K_{u,1} (\mathbf{m}_1 \mathbf{u}_z)^2 + K_{u,2} (\mathbf{m}_2 \mathbf{u}_z)^2 = K_u \left((\mathbf{m}_1 \mathbf{u}_z)^2 + (\mathbf{m}_2 \mathbf{u}_z)^2 \right). \tag{S3}$$

Moreover, we have only consider intralattices interfacial Dzyaloshinkii-Moriya interaction (DMI), with the same constant D_i for both sublattices

$$\varepsilon_{dmi} = D_1 \left((\mathbf{m}_1 \cdot \mathbf{u}_n) \nabla \cdot \mathbf{m}_1 - \mathbf{m}_1 \cdot \nabla (\mathbf{m}_1 \cdot \mathbf{u}_n) \right) + D_2 \left((\mathbf{m}_2 \cdot \mathbf{u}_n) \nabla \cdot \mathbf{m}_2 - \mathbf{m}_2 \cdot \nabla (\mathbf{m}_2 \cdot \mathbf{u}_n) \right), \tag{S4}$$

being $\mathbf{u}_n$ the vector normal to the interface inducing DMI, which is $\mathbf{u}_z$ in the case study as shown in Fig. S1(a).

Finally, there are three contributions to the exchange interaction, as sketched in Fig. S1(b). The intralattice (FM) exchange interaction *between adjacent cells*, with (non-local) intralattice exchange constants A_{ii}, and A_{jj}. We have assumed the same value for both sublattices. The interlattice (AFM) exchange constant *between adjacent cells*, with non-local interlattice exchange constant A_{ij}. And finally, the interlattice (AFM) exchange constant within a micromagnetic cell, with local interlattice exchange constant B_{ij}. Therefore, the exchange energy density is read

$$\varepsilon_{exch} = A_{ii} ||\nabla \mathbf{m}_1||^2 + A_{ii} ||\nabla \mathbf{m}_2||^2 + A_{ij} \langle (\nabla \mathbf{m}_1), (\nabla \mathbf{m}_2) \rangle + B_{ij} \mathbf{m}_1 \mathbf{m}_2, \tag{S5}$$

with $||M||$ the Frobenius norm of matrix M and $\langle M_1, M_2 \rangle$ the Frobenius inner product of matrices M_1, and M_2. The corresponding effective field is

$$\mathbf{H}_{eff,i} = \frac{2K_{u,i}}{\mu_0 M_{s,i}} m_{z,i} \mathbf{u}_z + \frac{2D}{\mu_0 M_{s,i}} \left(\nabla (\mathbf{m} \cdot \mathbf{u}_n) - (\nabla \cdot \mathbf{m}) \mathbf{u}_n \right) + \frac{2A_{ii}}{\mu_0 M_{s,i}} \nabla \cdot (\nabla \mathbf{m}_1) + \frac{A_{ij}}{\mu_0 M_{s,i}} \nabla \cdot (\nabla \mathbf{m}_2) + \frac{B_{ij}}{\mu_0 M_{s,i}} \mathbf{m}_2 \tag{S6}$$

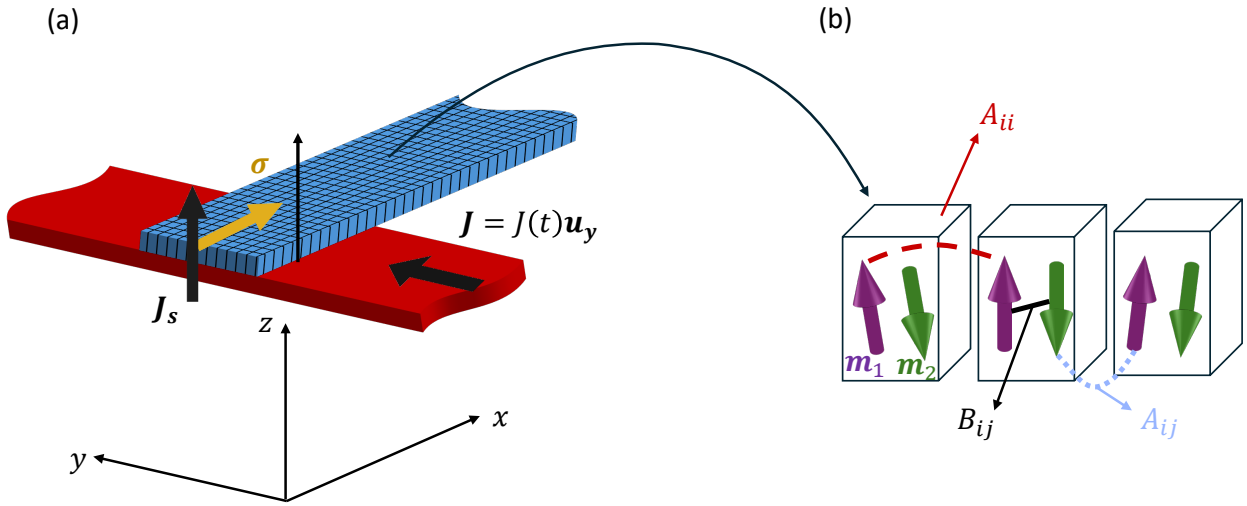

FIG. S1. (a) Scheme of the system under consideration with the reference frame and the micromagnetic mesh. (b) Sketch of the micromagnetic cell highliting the two sublattices consider in the model and the three contributions between them: local interlattices exchange B_{ij} in black, non-local intralattice exchange A_{ii} in red, and non-local interlattices exchange A_{ij} in blue.

Although no random noise has been considered, temperature effects have been taking into account by a temperature dependent magnetization saturation given by Eq. 2. In order to numerically solve these couple LLG equation we have to discretize our sample in finite but small micromagnetic cells. Additionally, we need to give realistic values for all the involve parameters. Those values are reported in the main text and can be found in the literature[11,16,18–23].

An additional comment must be made on the discretization scheme used to perform the simulations. As it has been stated in the main text, our micromagnetic code solves (S1) by a finite difference method. The computational region has been discretized in 1 nm $\times$ 1 nm $\times$ 6 nm cells. This choice has been made according to two main objectives. The first is to have sufficient spatial resolution for the spin waves taking into account the excitation frequency spectrum of the system (up to 1 THz). The second is to reduce the computational cost of the simulations without affecting the coherence of the results. In this sense, it has been considered that the system does not present variations in the magnetization in the thickness of the strip. Accordingly, the dimension of each cell in the Z axis has been made to coincide with the thickness of the strip, so that only one single cell is considered along this axis. To check the validity of this approach, the simulations shown in Fig.2(b) have been repeated, but dividing the strip thickness into two cells of 3 nm height and three cells of 2 nm height. The results are shown in Fig. S2, where it can be seen that the dispersion diagrams obtained using different number of cells in thickness present identical dependencies with the wavevector.

S2 Dispersion Relations and Group Velocity at Very High Coupling Regime

In this section we provide with additional dispersion relation results when the local interlattice exchange constant is increased up to $B_{ij} = -90\frac{\text{MJ}}{\text{m}^3}$, i.e., one order of magnitude larger than the value used in the main text. Results in every temperature scenario explored in the main text, that is, $T = 200$ K (below T_A), $T_A = 260$ K, and $T = 300$ K (above T_A), are also shown. The section is completed with group velocity graphs for the cases under study.

Dispersion relation diagrams for different local interlattice exchange values are shown in Fig. S3. Each row corresponds to a different B_{ij} so that $B_{ij} = -90\frac{\text{MJ}}{\text{m}^3}$ for the top row, $B_{ij} = -45\frac{\text{MJ}}{\text{m}^3}$ for the middle row and $B_{ij} = -9\frac{\text{MJ}}{\text{m}^3}$ for the bottom row. Additionally, each column corresponds to a different simulation temperature, i.e, temperature below T_A for the leftmost column, equal to T_A for the middle column, and above T_A for the rightmost column. The graphs here presented represent only a subset of all the simulated values, but allow us to confirm the conclusions drawn in the main text even in cases of strong coupling between sublattices. A conspicuous effect of the increase of the local interlattice exchange is the continuous growth of the splitting of the dispersion curves associated with each sublattice, which reveals that, indeed, the system should not be analyzed in general as two isolated FMs. Importantly, results reinforce the discrepancies between our simulations and the analytical expression (3) resulting from Kalinikos and Slavin's theory[27] mentioned in the main text as the coupling between sublattices is increased. The curves resulting from this analytical expression have been plotted on the same figure as dashed lines. In view of these discrepancies, we have opted for the fitting of the dispersion curves by means of biquadratic functions, in the form $f(k_x) = f_0 + ak_x^2 + bk_x^4$. The

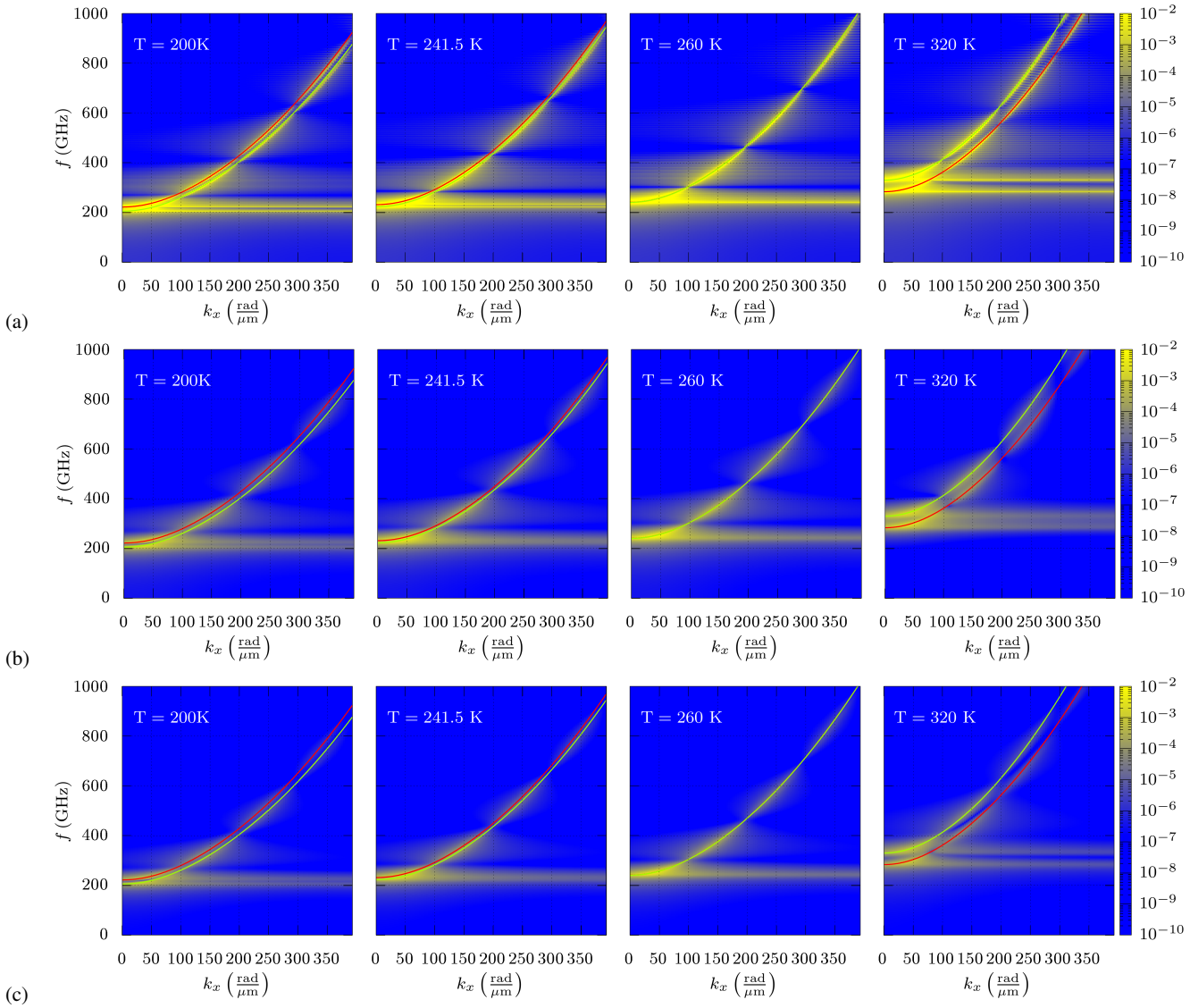

FIG. S2. Dispersion curves obtained for the FiM strip described in the main text, corresponding to Fig. 2(b) of the text, considering the same set of temperatures. The simulations have been performed taking different number of cells in the thickness of the system: (a) 1 cell of 6 nm, (b) 2 cells of 3 nm and (c) 3 cells of 2 nm. A pair of continuous lines, red and green, have been drawn on the dispersion diagrams as a guide for the eye. For each temperature considered, the lines drawn in (a), (b) and (c) are identical.

corresponding fitting curves have been also superimposed on the graphs as continuous lines, showing a much better agreement. These fittings highlight two sources of discrepancies, one related to temperature, probably due to a non-compensation of the angular momentum of the two sublattices, and the other due to an underestimation of the k^2 coefficient of the fitting compared to the that of (3) in the main text. As could be checked by comparing the fitting to a quadratic function such as (3), the uniform mode computed away from the angular momentum compensation point turns out to be underestimated for one subgrid and overestimated for the other, and the differences increase the further from the angular momentum compensation point. However, the underestimation of the k^2 term seems to be independent of the temperature with respect to T_A, since this coefficient is the same for all three temperatures shown at fix B_{ij}. The good agreement obtained with the biquadratic functions leads us to ponder whether the quadratic description of the dispersion curves given by the theory of Kalinikos and Slavin is sufficient to describe more complex systems, such as these coupled systems. Further theoretical work is therefore needed to adequately account for the effect of both local and non-local interlattice exchange in these materials, that could reveal the sources of the discrepancies.

In any case, to reinforce the need to use higher order terms than quadratic in the description of the dispersion curves, we have proceeded to obtain the corresponding group velocity curves. If the biquadratic or higher terms were irrelevant, the group velocities would deviate very little from the linear behavior versus the wave vector, but if the deviation is significant, this would

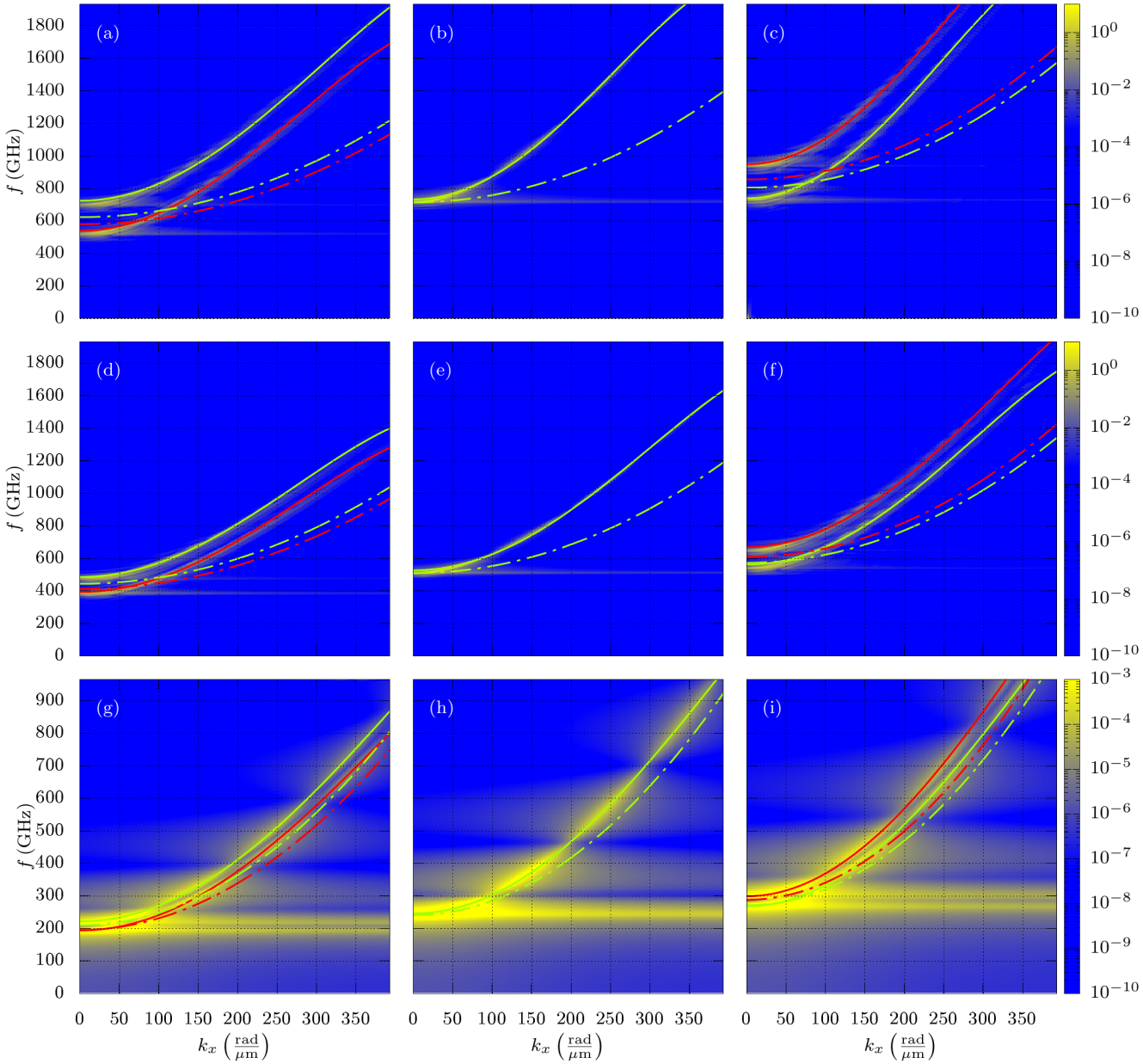

FIG. S3. Dispersion relation diagrams for different local interlattice exchange values and distinct temperatures. The taken B_{ij} values are: $B_{ij} = -90\frac{\text{MJ}}{\text{m}^3}$ for graphs (a), (b) and (c), $B_{ij} = -45\frac{\text{MJ}}{\text{m}^3}$ for graphs (d), (e) and (f)) and $B_{ij} = -9\frac{\text{MJ}}{\text{m}^3}$ for graphs (g), (h) and (i). The temperatures considered are: temperature below T_A for graphs (a), (d) and (g), equal to T_A for graphs (b), (e) and (h), and above T_A for graphs (c), (f) and (i). The resulting fitting of dispersion curves by means of biquadratic functions are also superimposed on the graphs.

be a clear indication of the need to include terms of higher order than quadratic in the description of magnon dynamics in these systems. In this sense, we have proceeded to derive the group velocity from the fitting curves in Fig. S3. The results are shown in Fig. S4, where the same criterion has been followed as in the previous figure when ordering the graphs (B_{ij} decreases from top to bottom and temperature goes from below T_A on the left to above T_A on the right, and is equal to T_A in the middle).

The plots show in general an initial linear growth of the group velocity as the magnon wavelength is reduced as expected from (3), with a very similar slope for both branches in cases where the temperature differs from T_A, but departing from this linear behavior to saturate when the wavelength is shortened sufficiently and decreasing for shorter wavelengths, thus showing a maximum group velocity at a finite k. Importantly, this behavior is extensible to the one curve in the case of a compensated material and is more pronounced as the coupling between sublattices increases. Nonetheless, is should be pointed out that these

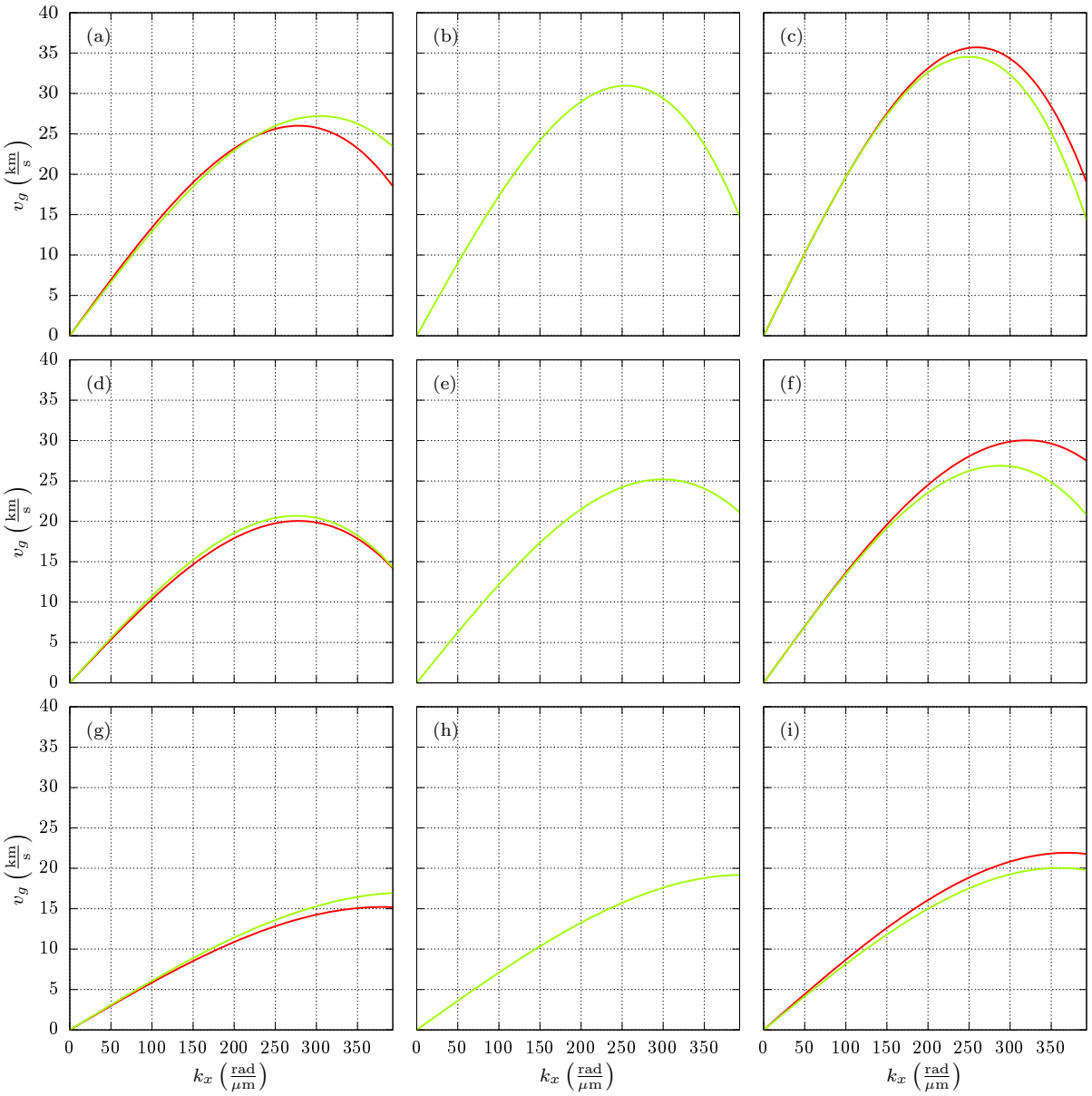

FIG. S4. Group velocity plots for different local interlattice exchange values and distinct temperatures. The taken B_{ij} values are: $B_{ij} = -90\frac{\mathrm{MJ}}{\mathrm{m}^3}$ for graphs (a), (b) and (c), $B_{ij} = -45\frac{\mathrm{MJ}}{\mathrm{m}^3}$ for graphs (d), (e) and (f)) and $B_{ij} = -9\frac{\mathrm{MJ}}{\mathrm{m}^3}$ for graphs (g), (h) and (i). The temperatures considered are: temperature below T_A for graphs (a), (d) and (g), equal to T_A for graphs (b), (e) and (h), and above T_A for graphs (c), (f) and (i).

surprising results are obtained from the fitting of the dispersion curves to a polynomial function. Thus, they can be affected by the truncation of the polynomial function and further theoretical work, which is out of the scope of the present study, would be required to clarify this behaviour. Finally, as might be expected from (3), group velocity increases with increasing (reducing) temperature (saturation magnetization).